Expanded View Figures

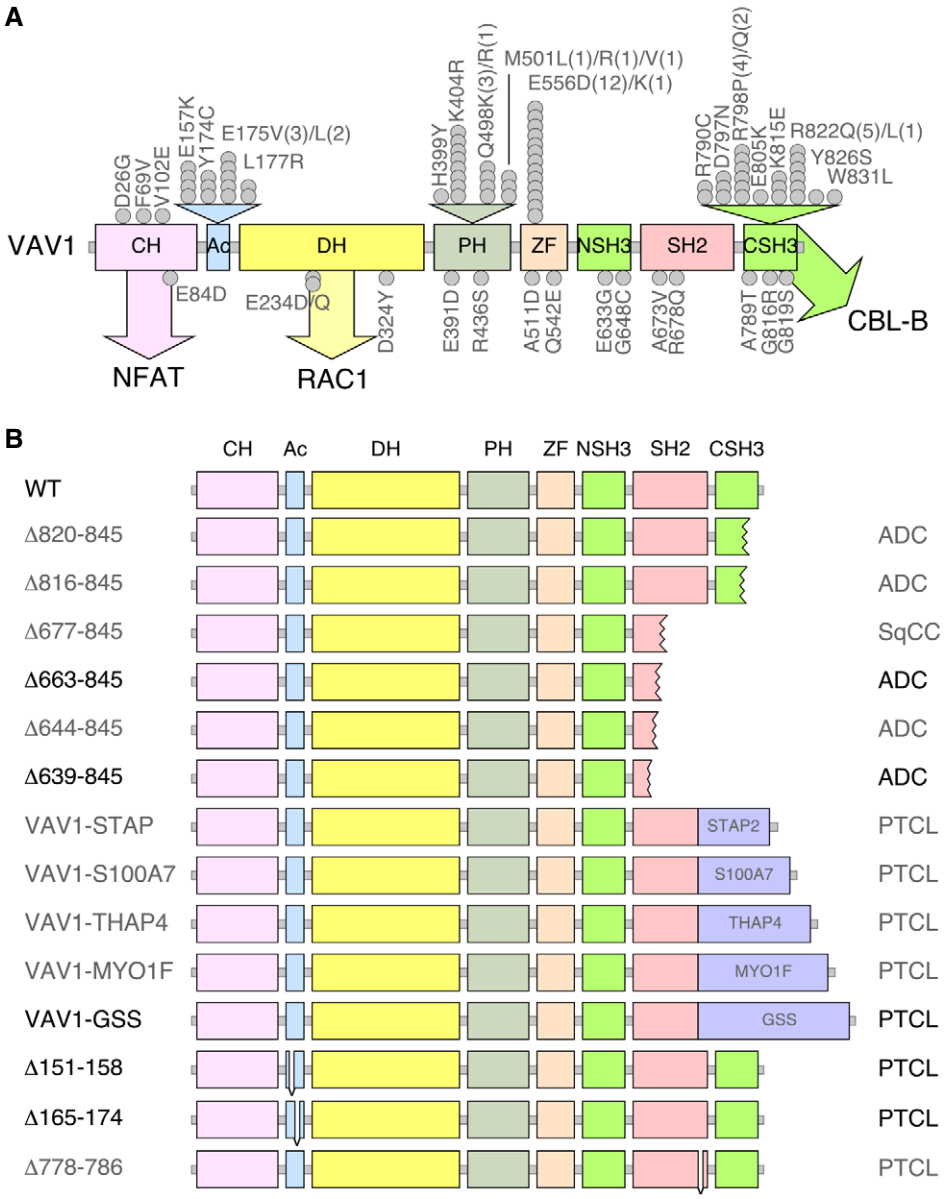

Figure EV1. Tumor-associated *VAV1* mutations.

A Localization of *VAV1* missense mutations identified in PTCL (top) and NSCLC (bottom) in the primary structure of the protein. Each dot represents one patient. Abbreviations for domains have been described in main text. Mutations analyzed in this study are shown in gray color. The main pathways activated by the VAV1 domains are indicated. CH, calponin homology; Ac, acidic; DH, Dbl homology; PH, pleckstrin homology; ZF, zinc finger; NSH3, most N-terminal SH3 domain; CSH3, most C-terminal SH3.

B Examples of C-terminal truncations (top, proteins 1 to 6), translocations affecting the C-terminal end (middle, proteins 7 to 11, fused protein indicated as a violet box), and internal gene deletions (bottom, proteins 12 to 14) found in human patients. Mutations analyzed in this study are shown in gray font. Those not tested are in black font.

Figure EV2. CSH3 mutations alter the interaction between VAV1 and binding partners.

A Co-immunoprecipitation of indicated Vav1 proteins with CBL-B in Jurkat cells ectopically expressing the indicated combinations of proteins (top). Amount of immunoprecipitated CBL-B was assessed by reblotting the same filter with antibodies to CBL-B (second panel from top). Expression of ectopic VAV1 proteins (third panel from top) and endogenous tubulin α (loading control, bottom panel) was determined by immunoblotting using aliquots of the total cellular lysates used in the immunoprecipitation step. The color code of the mutant residues follows the criteria used in Fig 1C and D.

B–D Representative examples of the interactions found in Jurkat cells among GST-tagged proteins fused to the indicated CSH3 versions of Vav1 and the endogenous CBL-B, Dynamin 2, and HNRNPK proteins. In all cases, the relative amount of bait used in the pull-down assays is shown in the fourth panel from top. Expression of the endogenous proteins was determined by immunoblotting using aliquots of the total cellular lysates used in the pull-down step. Asterisks in the second and fourth panels in the total cellular lysate panels pinpoint the CBL-B and HNRNPK immunoreactive bands from the previous immunoblot of the same filter, respectively. In (D), asterisk in the first panel in the pull-down panels indicates the Dynamin 2 band from the previous immunoblot of the same filter. Similar results were obtained in three additional experiments. GST-VAV1^{P833L}, negative control of interaction (it bears a mutation that inactivates the binding properties of the domain). The color code of the mutant residues follows the criteria used in Fig 1C and D.

E Summary of binding alterations found in the Vav1 CSH3 mutants. Proper binding is shown as green boxes and arrows. Lack of binding is shown as blue boxes and arrows. The activation of NOTCH1 signaling is depicted as a red box. The percentage of each mutant subclass (relative to all CSH3 mutants tested) is indicated at the top of each functional subgroup.

Source data are available online for this figure.

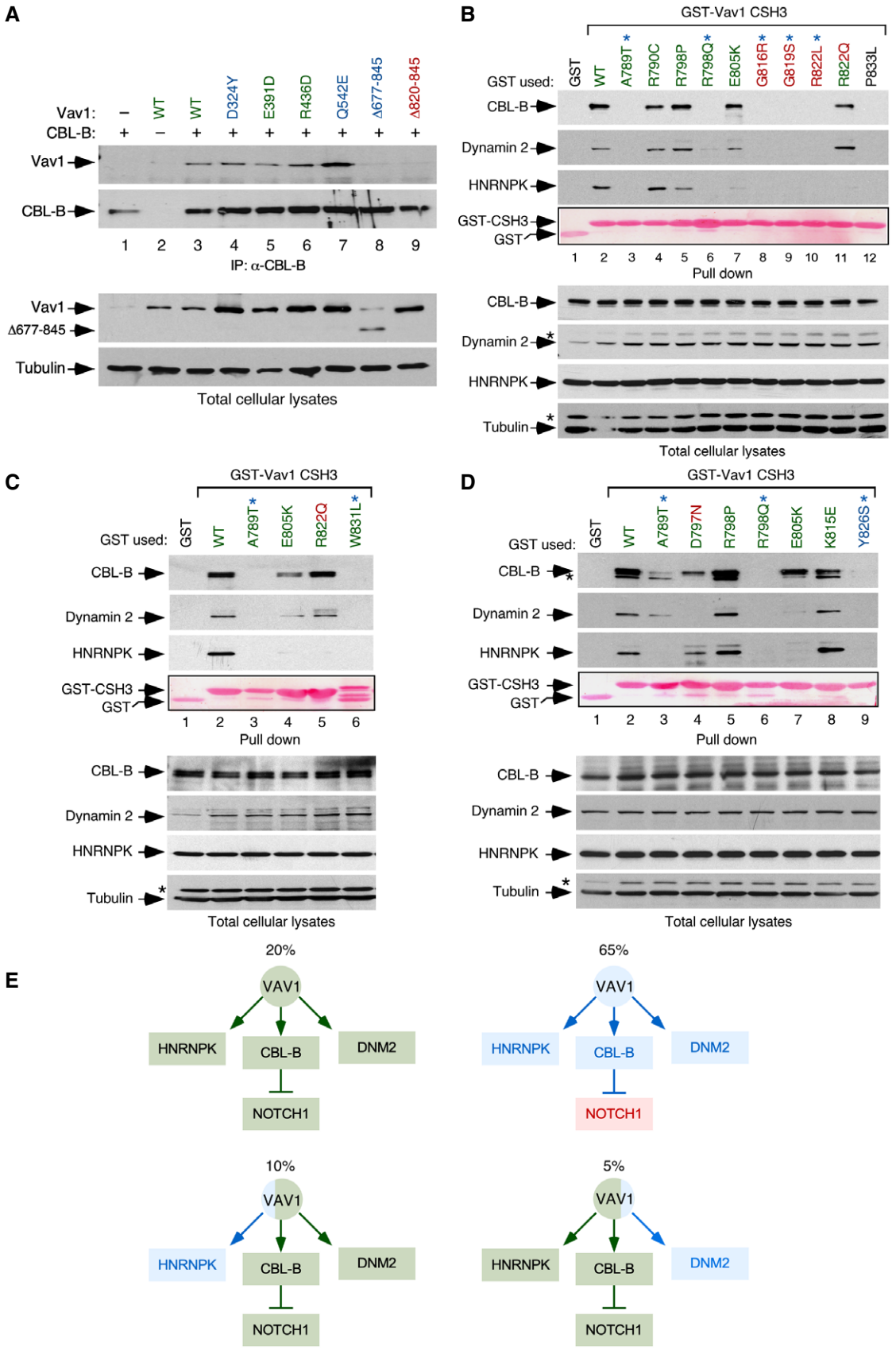

Figure EV2.

Figure EV3. New regulatory layers unveiled by the VAV1 mutations.

A Depiction of the main intramolecular interactions that mediate the inactivation of VAV family proteins in the nonphosphorylated state. The interactions of the CH, Ac, and CSH3 domains with the catalytic cassette are shown in pink, blue, and purple lanes, respectively. The phosphorylation sites involved in the activation step are indicated. PTKs, protein tyrosine kinases involved in the tyrosine phosphorylation-mediated activation step of VAV family proteins.

B, C Depiction of areas of interaction between the CH-Ac and the catalytic cassette. The side chains of the residues whose mutation leads to GOF effects are shown in red. The main regulatory phosphosites are shown in blue. The CH, Ac, and DH region are colored in purple, blue, and yellow, respectively.

D, E Depiction of the area of the catalytic cassette containing the α_{11} DH helix, the PH, and the ZF regions in the context of the crystallized CH-Ac-DH-PH-ZF (D) and the CH-PH-ZF (E) fragments of human and mouse Vav1, respectively. Residues whose mutation leads to GOF and LOF effects are colored in red and blue, respectively. The CH, Ac, DH, PH, and ZF regions are colored in purple, blue, yellow, green, and brown, respectively.

F Zoom of the Vav1 α_{11} DH helix-PH-ZF region showing the interactions established by the indicated residues. Residues and domains are depicted as in above panels.

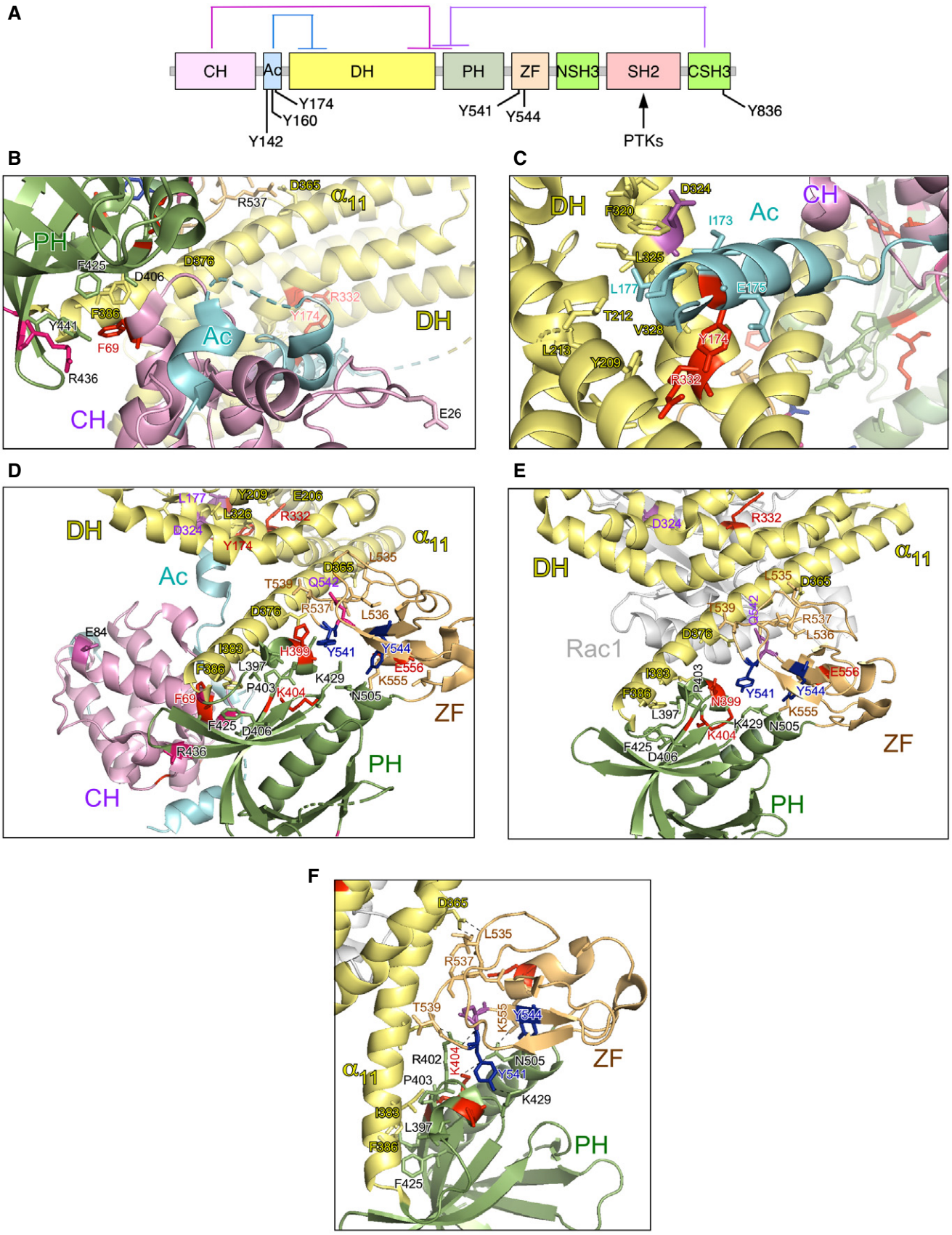

Figure EV3.

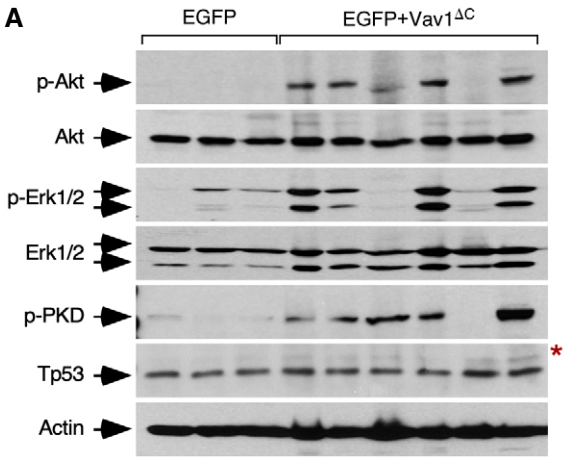

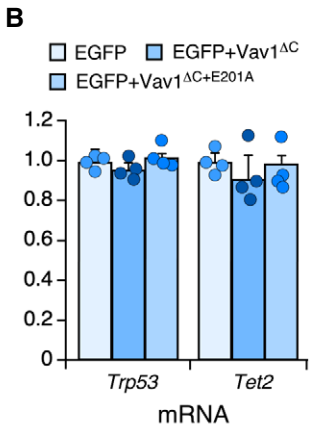

Figure EV4. Status of signal transduction pathways in Vav1$^{\Delta C}$-transformed cells.

A Western blot showing the levels of phosphorylated and total proteins in spleen extracts from control and tumor-bearing recipient mice that had been transplanted with the indicated retrovirally transduced CD4$^+$ T cells (top). Total levels of Akt, Erk1/2, and actin were used as loading controls. The red asterisk indicates a panel that has been generated using an independent filter but the same tissue lysates.

B Abundance of indicated transcripts (bottom) in splenic cells from control (EGFP$^+$), tumor-bearing mice (expressing EGFP and Vav1$^{\Delta C}$), and mice transplanted with cells transduced with the catalytically dead version of Vav1$^{\Delta C}$ (expressing EGFP and Vav1$^{\Delta C+E201A}$). Values are given relative to the expression of each transcript in samples obtained from EGFP controls (which was given an arbitrary value of 1). $n = 4$ animals per class analyzed. a.u., arbitrary unit. Data represent the mean ± SEM. Statistical values obtained using the Student's t are given relative to control EGFP$^+$ cells.

Source data are available online for this figure.

Figure EV5. Vav1$^{\Delta C}$ triggers a vast proliferative program in transformed T$_{FH}$ cells.

A Main functional pathways upregulated in the Vav1$^{\Delta C}$-dependent transcriptome according to unbiased GSEAs. For all of them, q-val < 0.05.

B Principal component analysis showing the enrichment of the Vav1$^{\Delta C}$-dependent signature across the indicated tumor-associated transcriptomes. cSCC, cutaneous squamous cell carcinoma; oSCC, oral squamous cell carcinoma; T-ALL, T-cell acute lymphoblastic leukemia.

C GSEA for the Vav1$^{\Delta C}$-tumor gene expression matrix using as gene set the differentially expressed genes by the FOXO pathway. The expression profile of the top 25 leading-edge genes in the transcriptome of CD4$^+$ T cells from healthy and Vav1$^{\Delta C}$ tumor-bearing mice is shown. The normalized enrichment scores (NES) and false discovery rate values (FDR, using q values) are indicated inside the GSEA graph. Relative changes in abundance are shown in color gradients according to the color scale shown at the bottom. q-val, q value.

D GSEAs for the Vav1$^{\Delta C}$-tumor gene expression matrix using as gene set the differentially expressed genes by the SJL mouse model. The NES and FDR (using q values) are indicated inside the GSEA graph as in C. q-val, q value.

E Dot plot of the Vav1$^{\Delta C}$-dependent gene signature fit score in the indicated experimental groups (bottom). Dots represent values from an individual sample. Bars represent the mean enrichment value ± SEM for the overall sample set. ***$P \leq 0.001$ (according to Tukey's honest significance difference test).

F Main functional categories encoded by the Vav1$^{\Delta C}$-specific gene subset described in the main text. Up (red); down (blue). For all of categories, $P \leq 0.001$ (Fisher's exact test).

G Fraction of the upregulated (left) and downregulated (right) Vav1$^{\Delta C}$-driven transcriptome showing conservation with the expression programs identified in human AITL patients. Relative changes in abundance are shown in color gradients according to the color scale shown on the right. Healthy, CD4$^+$ T cells from healthy patients (green box). AITL, human AITL (red color boxes).

H Venn diagrams representing the number of up- (top) and downregulated (bottom) genes from the Vav1$^{\Delta C}$-dependent transcriptome that are shared with the AITL patient dataset used in panel G.

I Enrichment of indicated Vav1$^{\Delta C}$-driven gene signatures that are shared with the AITL patient dataset used in panel G.

J Heatmaps showing the expression profiles of human and mouse differentially expressed genes (DEG) belonging to the indicated functional categories (indicated on the left of each panel). Each row represents 1 DEG identified in the indicated AITL models (top). Each column represents 1 sample. The number of genes of each functional category is indicated. Relative changes in abundance are shown in color gradients according to the color scale shown on the bottom right. Green boxes, healthy individuals (in the case of human data), and WT mice. Red boxes, AITL samples from either patients or the indicated mouse models.

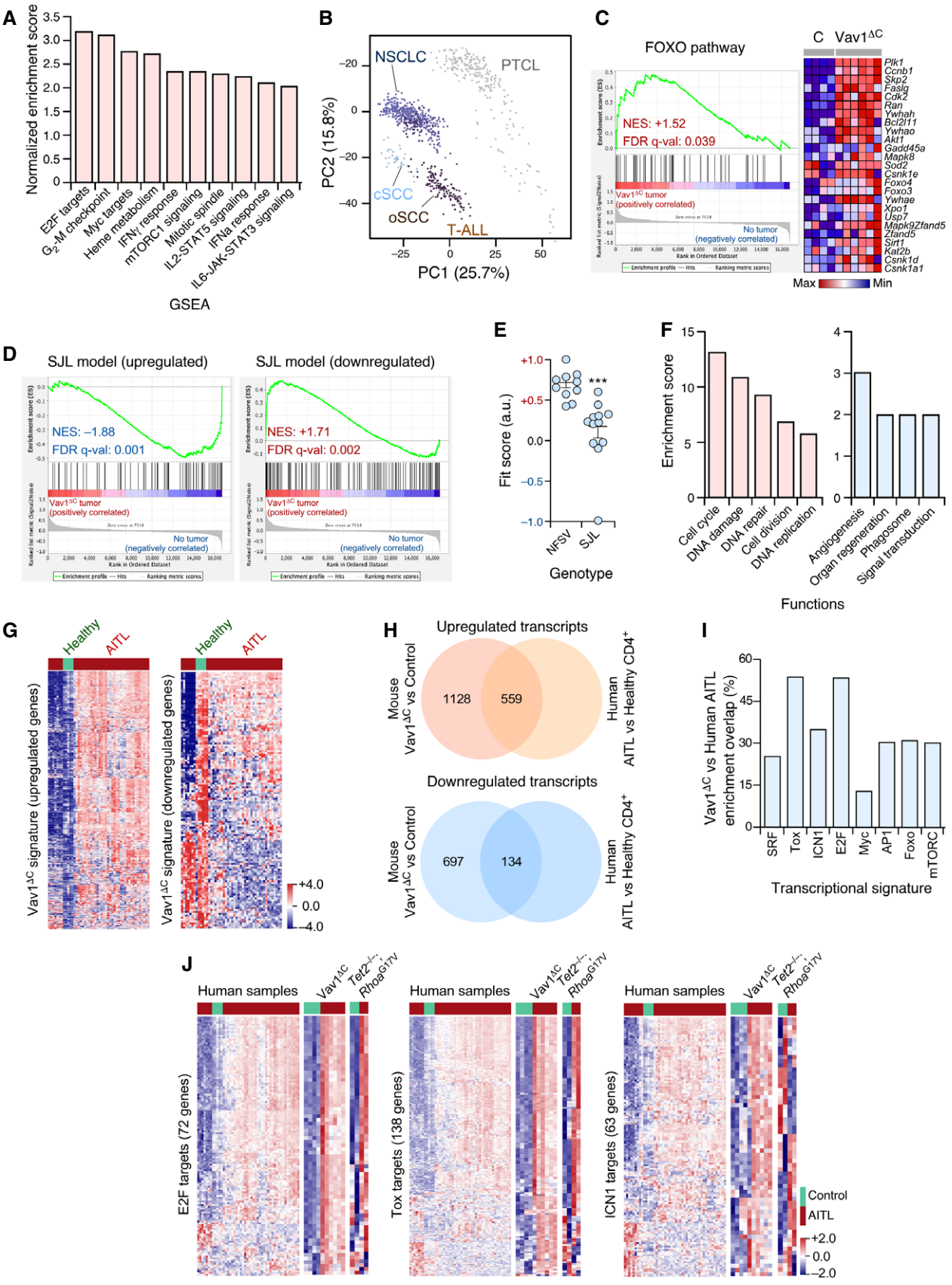

Figure EV5.